Fiber-Optic Remoting of an Ultrahigh Dynamic Range Radar

J. E. Román, L. T. Nichols, K. J. Williams, *Member, IEEE,* R. D. Esman, *Senior Member, IEEE,* G. C. Tavik, M. Livingston, and M. G. Parent

***Abstract*— We demonstrate, for the first time, fiber-optic remoting of an X-band radar with ultrahigh dynamic range, and show that photonic components can meet the stringent phase noise requirements for remoting modern radars. Fiber optic links were designed and built to remote the antenna and transmitter of the AN/SPQ-9B Advanced Development Model radar. The remoting links tested successfully in both transmit and receive configurations without significantly degrading the measured, postintegration, 87-dB signal-to-noise ratio of the radar. The results show the potential of photonic technology to remote the transmitter/receiver modules of active array radars.**

***Index Terms*—Active array antennas, fiber-optic remoting, optical fiber delay lines, transmitter/receiver modules.**

I. Introduction

ONE OF THE fundamental advantages of optical fiber over RF cable in the processing of microwave signals is the low signal loss per unit length [1]. This property makes fiber optics ideal for remoting microwave systems such as the transmitter/receiver (T/R) module of a radar. From the microwave perspective, however, remoting an antenna and its transmitter is not a trivial task. A typical radar T/R module requires several watts of RF power from its transmitter, which means that the remoting fiber-optic link (FOL) must be able to handle high RF powers without saturation. In addition, modern radar systems have stringent phase noise requirements, hence any additional phase noise introduced by the photonic components may degrade the radar's sensitivity. These issues have raised the question of whether photonic technology is well-suited for remoting modern radars with high dynamic range. To date, however, there have been no published experimental results to date to validate or dismiss such concerns.

In this paper, we demonstrate, for the first time, fiber-optic remoting of an X-band radar, and in the process, we show that photonic technology can meet the stringent phase noise requirements for remoting modern radars. Fiber-optic links were designed and built to remote the antenna and transmitter of the AN/SPQ-9B Advanced Development Model (ADM) radar in both transmit and receive configurations. This radar was chosen because it has a high dynamic range (75 dB over 1.3 MHz bandwidth) and its nominal 90-dB post integration signal-to-noise ratio (SNR) provided a stringent phase noise test for a photonic link in a remoting application. The results presented here demonstrate the feasibility of photonic technology for remoting active arrays.

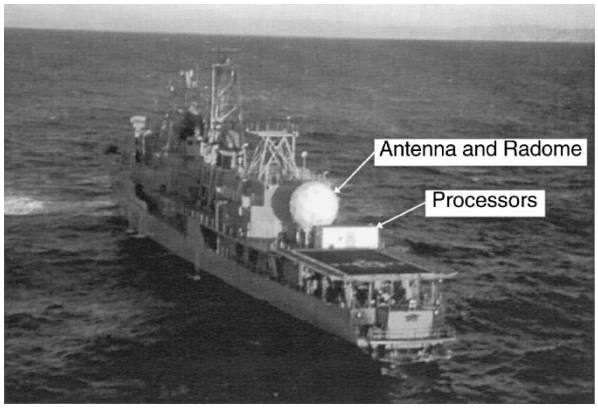

Fig. 1. AN/SPQ-9B ADM radar shown here aboard the Self Defense Test Ship, Port Hueneme, CA.

The paper is divided into five sections. In Section II, the operation and specifications of the AN/SPQ-9B ADM radar are described. In Section III, the FOL requirements are derived for both the transmit and receive configurations. The designs for the transmit and receive FOL's are described and the measured frequency response and phase noise characteristics are presented. In Section IV, the remoting links are tested in the AN/SPQ-9B ADM radar and the results are presented. Finally, Section V summarizes results.

II. Operation of AN/SPQ-9B ADM Radar

The AN/SPQ-9B ADM radar, shown in Fig. 1, is a pulsed, Doppler-processing, X-band, horizon search radar designed for operation on Naval surface ships. Its main function is the detection of low-flying aircraft and sea-skimming missiles. Detection of these targets is difficult because their presence is masked by the strong scattering from sea and land clutter. By utilizing RF components with low phase-noise, this radar achieves up to 90-dB clutter cancellation. It has the highest dynamic range of any existing modern radar.

Fig. 2 shows a simplified schematic diagram of the AN/SPQ-9B ADM radar. The system can be divided into six

Manuscript received March 24, 1998; revised August 12, 1998. This work was supported by the Office of Naval Research.

J. E. Román, L. T. Nichols, K. J. Williams, and R. D. Esman are with the Naval Research Laboratory, Code 5672, Washington, DC 20375 USA.

G. C. Tavik and M. Livingston are with the Naval Research Laboratory, Code 5327, Washington, DC 20375 USA.

M. G. Parent is with the Naval Research Laboratory, Code 5317, Washington, DC 20375 USA.

Publisher Item Identifier S 0018-9480(98)09202-3.

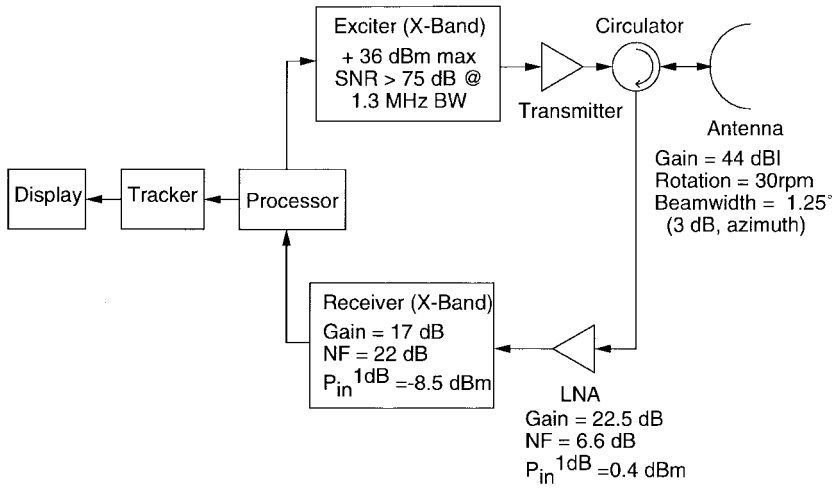

Fig. 2. AN/SPQ-9B ADM radar simplified block diagram.

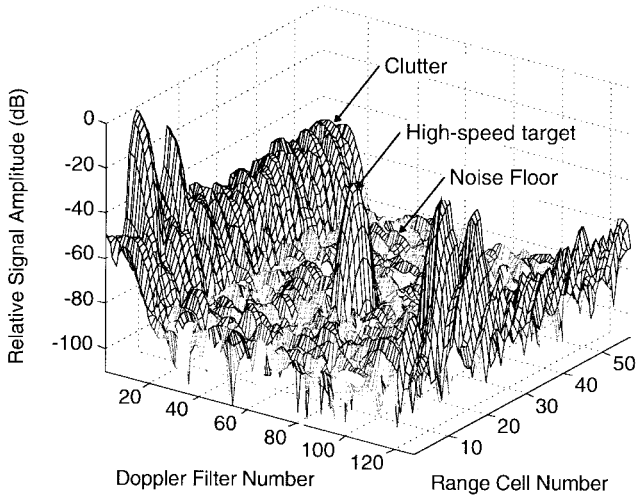

Fig. 3. Range/Doppler plot.

main components: a rotating antenna, an exciter, a transmitter, a receiver, a low-noise amplifier (LNA), and a processor. The antenna is a parabolic torus dish rotating at 30 rpm with a gain of 44 dBi and a one-way 3-dB beamwidth of 1.25° in azimuth. The exciter operates at X-band with a maximum output power of +36 dBm and an SNR greater than 75 dB over a 1.3 MHz noise bandwidth. The receiver has a gain of 17 dB, a noise figure of 22 dB, and a 1-dB input compression point of −8.5 dBm. The LNA has a gain of 22.5 dB, a noise figure of 6.6 dB, and a 1-dB input compression point of +0.4 dBm. These gains and noise figures include all loses due to transmission lines and other RF components.

The basic operation of the AN/SPQ-9B ADM radar can be described as follows. Multiple pulses are transmitted with a given pulse repetition interval (PRI) to measure the relative phase change from pulse to pulse due to the Doppler shift caused by a moving target. After reaching steady-state conditions, N return pulses or "echoes" are received, converted to baseband, and digitized to generate the range/Doppler plot of Fig. 3, showing range (target distance) on the x-axis, Doppler (target velocity) on the y-axis, and signal power on the z-axis. Since low-velocity clutter has a different Doppler shift than high-speed targets, the frequency of the returned pulses can be used to discriminate between the two. The radar's sensitivity is then determined by the thermal noise floor of the LNA (ref Fig. 2).

Some basic details of interpreting the range/Doppler plot are as follows. The mth row of the range/Doppler plot corresponds to a target distance, r_m, given by

$$r_m = \frac{c\tau_m}{2}, \qquad m = 1, 2, \cdots, M \tag{1}$$

where c is the speed of light and τ_m is the round-trip time delay for an echo scattered from the mth range cell

$$\tau_m \approx \frac{(m-1)T_{\mathrm{PRI}}}{M-1} + kT_{\mathrm{PRI}} \tag{2}$$

where T_{PRI} is the PRI, M is the total number of range cells (rows), and k is a nonnegative integer. The second term on the right represents range ambiguity arising from the relatively short PRI. In this work, the pulse width was 1.2 μs and the PRI was 50.4 μs, giving an unambiguous target detection range $(k = 0)$ of 7.56 km. Targets located farther than this range are aliased into the range/Doppler plot, corresponding to values of $k > 0$ in (2).

The nth column of the range/Doppler plot corresponds to a Doppler frequency, f_n, given by

$$f_n = \frac{1}{T_{\mathrm{PRI}}}\frac{(n-1)}{N} + k\left(\frac{1}{T_{\mathrm{PRI}}}\right), \qquad n = 1, 2, \cdots, N \tag{3}$$

where N is the number of pulses received and k is any integer. The second term on the right-hand side of (3) represents the ambiguity in the velocity measurement.

The Doppler frequency, f_n, is also related [2] to the radial velocity of the target, v_n, by

$$f_n = \frac{2v_n f_c}{c} \tag{4}$$

where f_c is the frequency of the transmit signal (X-band for the AN/SPQ-9B ADM radar). Thus, the nth column

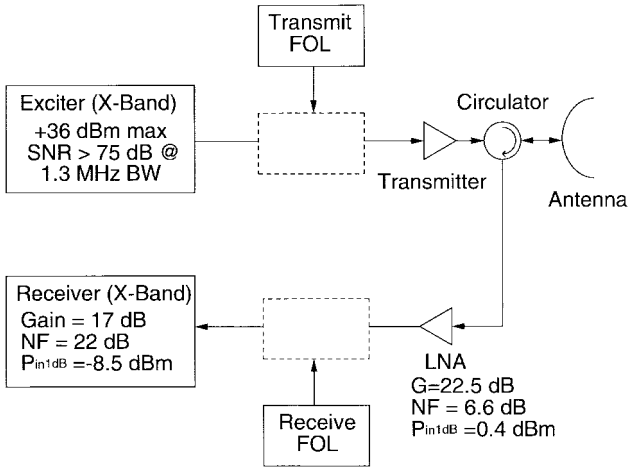

Fig. 4. AN/SPQ-9B ADM system diagram with remoting FOL's.

TABLE I
SPECIFICATIONS FOR REMOTING FOLS

Specifications @ X-Band	Transmit FOL	Receive FOL
Length (m)	40	40
Gain (dB)	0	0
Noise Figure (dB)	< 58*	< 22
1-dB Input Compression (dBm)	> 36	> -8.5
Phase Noise @ f > 1 MHz (dBc/Hz)	< -145	< -145

* Specified for 90-dB SNR @ 1.3 MHz bandwidth.

corresponds to a radial target velocity given by

$$v_n = \frac{c}{2T_{\mathrm{PRI}} f_c}\left(\frac{(n-1)}{N} + k\right), \quad n = 1, 2, \cdots, N; \quad k = \text{integer} \tag{5}$$

The above formulas will be helpful in interpreting the remoting test results of Section IV.

III. DESIGN AND CHARACTERIZATION OF FIBER-OPTIC LINKS

Fig. 4 shows the placement of the remoting fiber-optic links within the AN/SPQ-9B ADM system. This particular positioning of the FOL's was chosen to resemble that required for remoting a typical T/R module. This configuration would allow placement of each T/R module's receiver (downconverter) and exciter (upconverter) below deck, where constraints on the size and weight of these items can be relaxed. Although longer remoting distances were possible, 40 m was chosen as a reasonable distance to demonstrate the technique. Table I shows the specification requirements for the FOL's. The gain, noise figure, and 1-dB compression specifications were chosen to preserve those of the exciter and the receiver. The phase noise specification was determined from the measured phase noise of the stabilized local oscillator (STALO) shared by the exciter and the receiver, which is shown in Fig. 5.

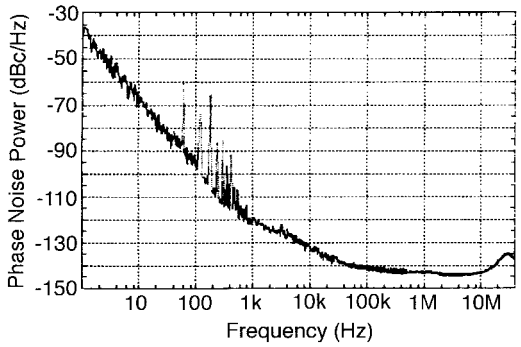

Fig. 5. Measured phase noise power spectrum for STALO of AN/SPQ-9B ADM radar.

Fig. 6 shows the transmit and receive fiber-optic links designed and built to remote the AN/SPQ-9B ADM radar. The remoting links consisted of a fiber-optic delay line (FODL) followed and/or preceded by microwave amplifiers and attenuators. The microwave amplifiers were used to compensate for the 30–40-dB RF loss of the FODL's. Two different FODL's were used, one based on external modulation (XMOD) of a solid-state laser [Fig. 6(a)], and one based on direct modulation (DMOD) of a high-speed distributed feedback (DFB) laser diode [Fig. 6(b)].

In the XMOD FODL, the RF signal was fed to the input of a $LiNbO_3$ Mach-Zehnder optical modulator (MZM). The MZM amplitude-modulated a 150-mW single-frequency diode-pumped fiber-pigtailed solid-state laser operating at 1319 nm. Although this laser provided more optical power than required for this application, it was chosen for its low relative intensity noise (RIN) of -165 dB/Hz. From basic noise figure considerations for a photonic link [3], it can be shown that such low RIN levels are required to meet the noise figure specifications of Table I. The RF-modulated optical signal was routed through 40 m of SMF-28 optical fiber to simulate the desired remoting distance, and the RF signal was recovered using a 10-mW 15-GHz photodetector (PD). The optical power of the laser was adjusted to produce a photodetector current of 5 mA at quadrature.

In the DMOD FODL, the RF signal directly modulated a 1550-nm DFB laser diode [4] having a RIN of -155 dB/Hz at X-band. The modulated optical signal was then routed through 40 m of dispersion-shifted (DS) fiber and detected with another 10-mW 15-GHz photodetector. In order to maximize the dynamic range of the link, the DFB laser diode was biased at 100 mA (one-half the maximum bias current) resulting in a photodetector current of 1.9 mA.

A. Transmit FOL's

In the transmit links, the $+36$-dBm RF signal from the exciter output was attenuated to protect the MZM and the DFB laser diode from damage. The photodetected RF signal was preamplified by a 6–18-GHz amplifier with 20-dB gain, 2.5-dB noise figure, and -11-dBm input compression point, followed by a 2–26-GHz power amplifier with 41-dB gain, 6-dB noise figure, and $+33$-dBm output 1-dB compression point. Suitable microwave attenuators were placed in the system to

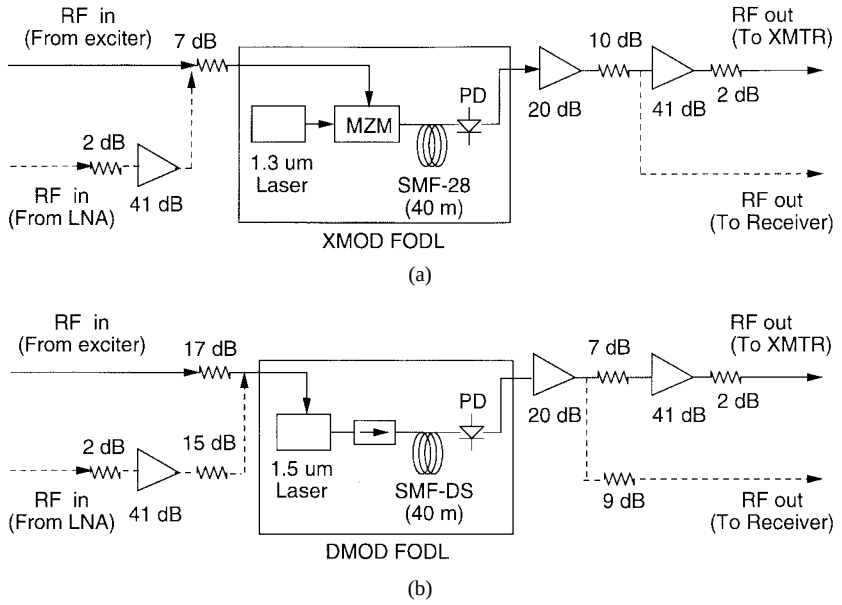

Fig. 6. Transmit and receive FOL's. (a) XMOD. (b) DMOD.

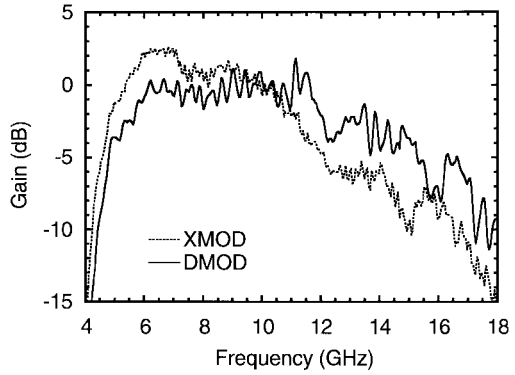

Fig. 7. Measured frequency response of transmit FOL's.

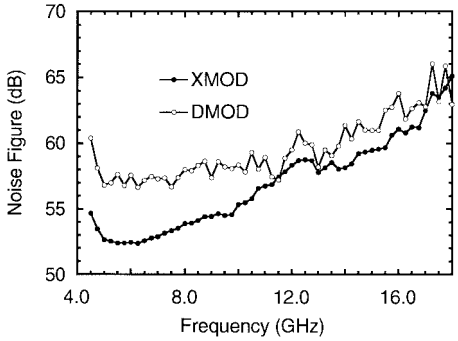

Fig. 8. Measured noise figure of transmit FOL's.

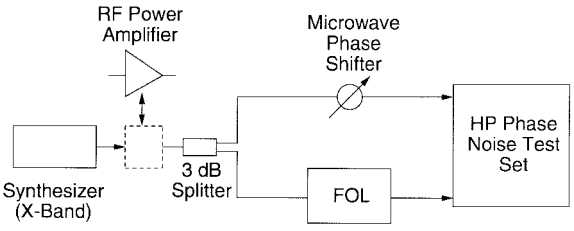

Fig. 9. Phase noise measurement apparatus.

achieve an overall system gain of 0 dB at X-band and avoid saturation of the 41-dB gain power amplifier.

Fig. 7 shows the measured frequency response for the transmit FOL's. As expected, both the external modulation and direct modulation links were lossless at X-band. The observed rolloff below 6 GHz was due to the 20-dB amplifier. The rolloff from 9 to 18 GHz in the XMOD FOL was due to the microwave amplifiers, the MZM, and the photodetector. We note that the fiber-optic links were not optimized for wideband operation because the AN/SPQ-9B ADM radar operates over a narrow frequency range. However, many of the associated RF components used in the links were capable of bandwidths in excess of 10 GHz, and proper selection of components would permit wideband operation.

Fig. 8 shows the measured noise figure for the transmit links. These were within the X-band specifications of Table I. No compression was observed in the DMOD FOL for RF inputs of up to 36 dBm. In the XMOD link, however, compression was observed at 29 dBm, which was below the specification of Table I. The lower compression point in the XMOD link was due to the MZM, which had a measured input 1-dB compression point of 22 dBm. The compression point could be raised by increasing the RF attenuation in front of the MZM, but doing this would result in a higher link noise figure; the configuration chosen provided a compromise between a low noise figure and a high-compression point.

The phase noise of the FOL's was measured using the apparatus shown in Fig. 9. An HP8340A synthesizer operating at X-band was split into two arms of an HP11848A phase detector, with the FOL in one arm and a phase shifter in the other arm to bias the phase detector at quadrature. For the transmit FOL's, a power amplifier was placed after the synthesizer to drive the FOL's close to compression with $+30$ dBm. Fig. 10 shows the measured phase noise power spectra for the transmit FOL's. Comparing these spectra with that of

TABLE II
SUMMARY OF MEASURED FOL CHARACTERISTICS

Specifications (X-Band)	Transmit			Receive		
	Spec.	Measured		Spec.	Measured	
		XMOD	DMOD		XMOD	DMOD
Gain (dB)	0	0.32	-0.85	0	0.06	-0.09
Noise Figure (dB)	< 58	54.5	58.5	< 22	16	18
1-dB Input Compression (dBm)	> 36	29	36	> -8.5	-10	-4
Phase Noise Power @ f > 1 MHz (dBc/Hz)	< -140	-145	-135	< -140	-140	-135

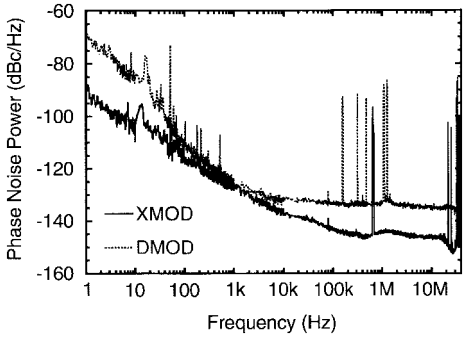

Fig. 10. Measured phase noise power spectrum for transmit FOL's.

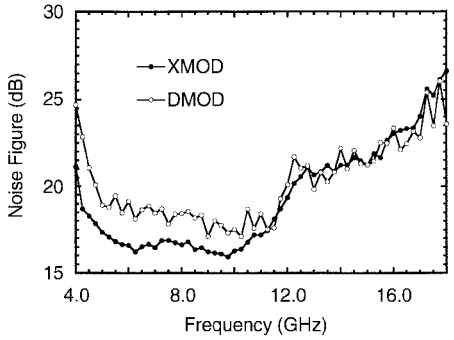

Fig. 11. Measured noise figure of receive FOL's.

Fig. 5, it was evident that the transmit FOL's would not add significant phase noise to the AN/SPQ-9B ADM system.

B. Receive FOL's

For the receive FOL's (Fig. 6), the input RF power from the LNA was relatively low. Therefore, the 41-dB gain power amplifier was moved to the front of the FOL. Since the power amplifier delivered up to +33 dBm, suitable attenuators were placed to protect the MZM and the DFB laser diode from damage. Additional attenuators were used to increase the input compression point and achieve lossless operation at X-band.

The measured frequency responses of the receive FOL's were similar to those shown in Fig. 7 for the transmit FOL's. Fig. 11 shows the measured noise figure of the receive FOLs; at X-band, these were well within the specifications of Table I. The measured input 1-dB compression points at X-band were -10 dBm for the XMOD link and -4 dBm for the DMOD link. Again, the lower compression point of the XMOD link was caused by compression in the MZM.

Fig. 12 shows the measured phase noise power spectra. These measurements were made using the apparatus of Fig. 9 without the power amplifier and driving the FOL's into compression with 10 dBm. Comparing the measured phase noise to that of the STALO (Fig. 5), it appeared the remoting FOL's would not increase the phase noise of the receiver. Table II summarizes the measured X-band characteristics of the FOL's.

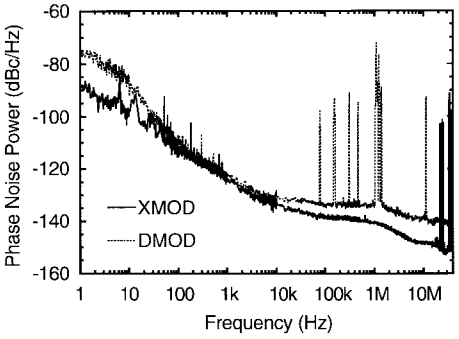

Fig. 12. Measured phase noise power spectrum for receive FOL's.

IV. SYSTEM TEST RESULTS

Once the FOL's were characterized, we tested their performance in the AN/SPQ-9B ADM radar. The tests were carried out at the NRL Chesapeake Bay Detachment in Chesapeake Beach, MD. The tests consisted of scanning the AN/SPQ-9B ADM antenna beam past a stationary target and measuring the ambiguous range/Doppler data with and without the FOL's inserted in the system. The target chosen was a corner reflector situated at Tilghman Island, MD, approximately 15.6 km from the radar. Each transmit and receive function was tested separately in order to assess its individual performance. For each function, three range/Doppler plots sets were recorded. One measurement was made without the FOL's and provided

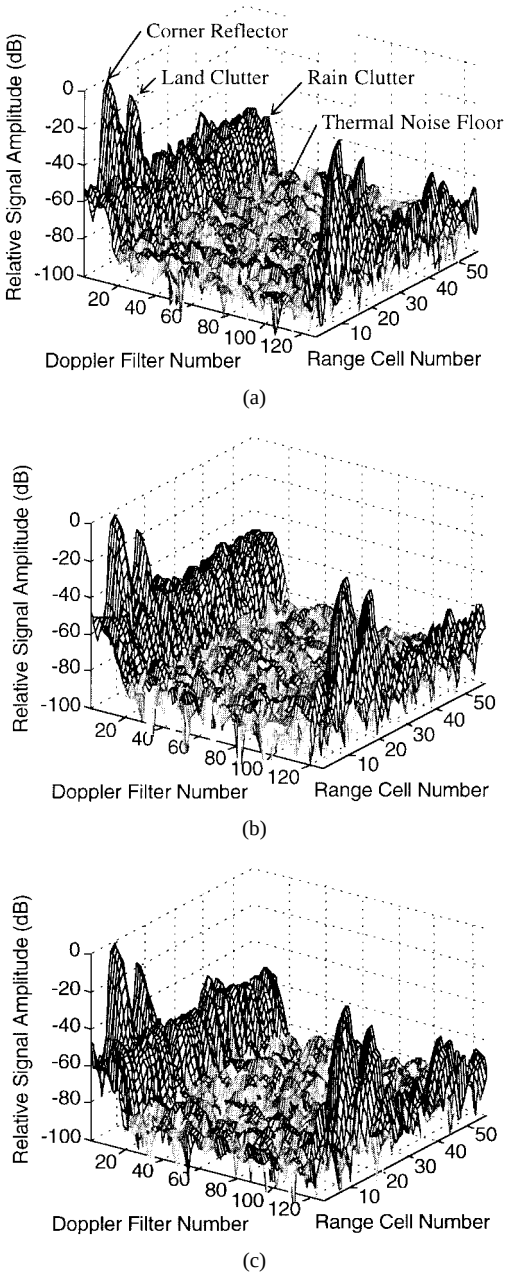

Fig. 13. Measured range/Doppler plots. (a) Transmit baseline (No FOL's). (b) Transmit XMOD FOL. (c) Transmit DMOD FOL.

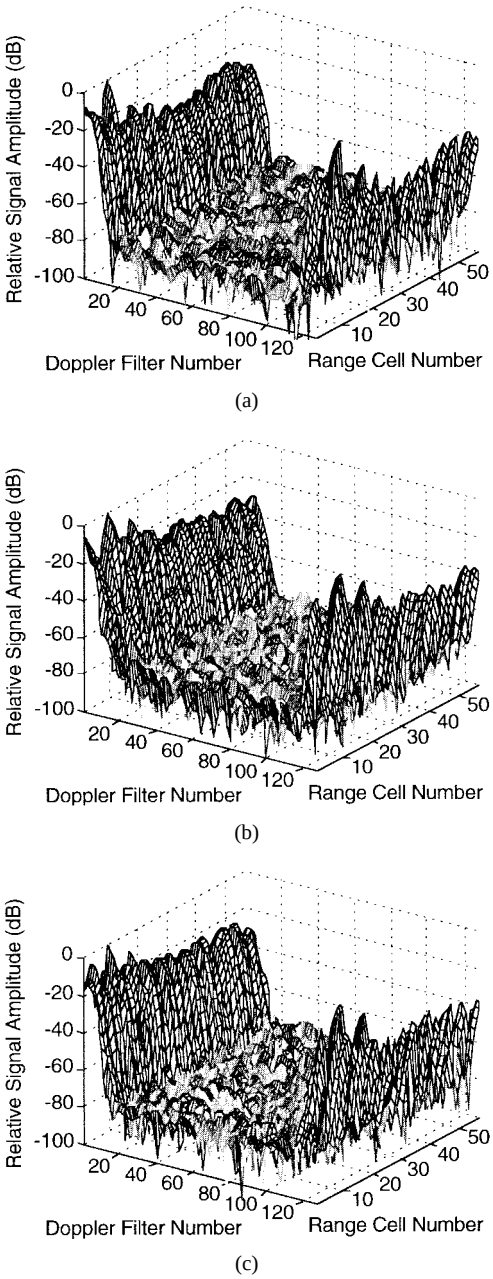

Fig. 14. Measured range/Doppler plots. (a) Receive baseline (NO FOL's). (b) Receive XMOD FOL. (c) Receive DMOD FOL.

the baseline. The other two measurements were made with the external-modulation and direct-modulation FOL's.

Fig. 13(a)–(c) shows the measured range/Doppler plots for the transmit tests. The baseline measurement [Fig. 13(a)] shows a main peak at range cell 9 corresponding to the corner reflector. In addition, a secondary peak representing land clutter can be clearly distinguished. The mean thermal noise floor for the baseline was -86.9 dB, 3 dB higher than the lowest achievable noise floor of -90 dB (postintegration) for this radar; variations in the baseline noise floor can approach ± 6 dB. The 3-dB reduction in SNR was due to the limited signal power received from the corner reflector, a consequence of the rainy conditions experienced during the test. Rain is evident in Fig. 13(a) by the echoes over all range cells at low Doppler values. Fig. 13(b) and (c) show the measured ambiguous data with the XMOD and DMOD transmission FOL's inserted, respectively. Both measurements were normalized with respect to the baseline peak for comparison. The figures show no significant degradation of the signal peak or noise floor for the DMOD FOL and a slight degradation in the signal peak for the XMOD FOL. Fig. 14(a)–(c) show the measured ambiguous data for the receive tests. Again, the results were normalized with respect to the baseline. No significant degradation in the signal peak or SNR is evident from these figures.

Table III compares the measured peaks and SNR's for all measurements. The baseline SNR was lower in the receive tests because these were made under heavy rain conditions, as evidenced by the large echoes over all range cells in Fig. 14.

TABLE III
SUMMARY OF AN/SPQ-9B ADM TEST RESULTS

	Transmit			Receive		
	Baseline	XMOD	DMOD	Baseline	XMOD	DMOD
Signal Peak (dB)	0	-1.7	-0.43	0	0.3	1.3
SNR (dB)	86.9	85.1	86.5	82.6	81.5	82.3

Notice that the peaks of these echoes are not centered at zero Doppler, thus indicating the radial velocity of rain.

The SNR's measured with the FOL's inserted were 0.3–1.8 dB lower than those measured for the baseline. For the DMOD FOL's, the SNR degradation was negligible (0.4 dB for transmit and 0.3 dB for receive). For the XMOD FOL's, however, the degradation was somewhat higher (1.8 dB for transmit and 1.1 dB for receive). The higher SNR degradation measured in the XMOD FOL's was caused by compression of the MZM. Again, this problem could be solved by increasing the RF attenuation in front of the MZM at the expense of a higher link noise figure.

V. CONCLUSION

We have successfully designed, built, and tested fiber-optic links to remote a high dynamic range X-band radar for the first time. The designed FOL's meet the performance specifications of the radar in terms of gain, noise figure, compression, and phase noise. In addition, the measured frequency response characteristics show the potential for wideband operation. When inserted in the AN/SPQ-9B ADM radar, the FOL's performed well in either receive or transmit configurations, showing no significant degradation of the system's baseline SNR.

These results demonstrate conclusively that photonic components can meet the stringent phase noise and SNR specifications of modern radars. This photonic technology is particularly well-suited for remoting active arrays because it allows placement of each T/R module's receiver (downconverter) and exciter (upconverter) below deck, where constraints of the size and weight of these items can be relaxed.

ACKNOWLEDGMENT

The authors thank Dr. P. J. Matthews for helpful comments on the phase noise measurements.

REFERENCES

[1] H. Zmuda and E. N. Toughlian, *Photonic Aspects of Modern Radar*. Boston, MA: Artech House, 1994.

[2] M. I. Skolnik, *Introduction to Radar Systems*. New York: McGraw-Hill, 1980, p. 68.

[3] L. T. Nichols, K. J. Williams, and R. D. Esman, "Optimizing the ultrawide-band photonic link," *IEEE Trans. Microwave Theory Tech.*, vol. 45, pp. 1384–1389, Aug. 1997.

[4] P. A. Morton, T. Tanbun-Ek, R. A. Logan, N. Chand, K. W. Wecht, A. M. Sergent, and P. F. Sciortino Jr., "Packaged 1.55 μm DFB laser with 25 GHz modulation bandwidth," *Electron. Lett.*, vol. 30, pp. 2044–2046, Nov. 1994.

J. E. Román, photograph and biography not available at the time of publication.

L. T. Nichols, photograph and biography not available at the time of publication.

K. J. Williams (S'86–M'89), photograph and biography not available at the time of publication.

R. D. Esman (S'82–M'85–SM'95), photograph and biography not available at the time of publication.

G. C. Tavik, photograph and biography not available at the time of publication.

M. Livingston, photograph and biography not available at the time of publication.

M. G. Parent, photograph and biography not available at the time of publication.